Received February 5, 2021, accepted February 28, 2021, date of publication March 9, 2021, date of current version March 16, 2021.

Digital Object Identifier 10.1109/ACCESS.2021.3064660

A Review of Fixed Switching Frequency Current Control Techniques for Switched Reluctance Machines

SUMEDH DHALE, (Student Member, IEEE), BABAK NAHID-MOBARAKEH, (Senior Member, IEEE), AND ALI EMADI, (Fellow, IEEE)

McMaster Institute for Automotive Research and Technology, McMaster University, Hamilton, ON L8P 0A6, Canada

Corresponding author: Sumedh Dhale (dhales@mcmaster.ca)

This work was supported in part by the Natural Sciences and Engineering Research Council of Canada (NSERC).

ABSTRACT By the virtue of its highly nonlinear magnetic characteristics, the Switched Reluctance Machine (SRM) poses a formidable challenge for digital current regulators operating at a fixed switching frequency. Very fast tracking performance demanded by highly dynamic reference current profiles often surpass the conventional limits on closed-loop bandwidth posed by finite sampling frequency. The non-linear nature of matched disturbance to be compensated by the controller appearing in the form of induced emf grows in significance as a function of operating speed while the varying nature of inductance profile stipulates a need for gain adaptation by the control law in order to maintain consistency in closed-loop dynamic response. In the view of these unique SRM characteristics, the paper presents a detailed theoretical analysis of the widely implemented current control techniques from literature and provides illustrations in the context of their implementation in a digital controller. The analysis presented in this paper can also serve as a foundation for more advanced versions of these control techniques as well as their combinations.

INDEX TERMS Current control, fixed switching frequency control, switched reluctance machines.

NOMENCLATURE

T_s, k, ω_s	Sampling time, instant and frequency
i_{ph}, $\hat{i}_{ph}$, i_{ref}, i_c	Phase current, its estimation, reference
ψ_{ph}, $\hat{\psi}_{ph}$, $\tilde{\psi}_{ph}$	Phase flux linkage, its measurement and its estimation error
d^*_{ph}, u^*_{ph}, u_{ph}	Controller output duty ratio, voltage, and phase terminal voltage
ϵ_{ph}, $\hat{\epsilon}_{ph}$, $\tilde{\epsilon}_{ph}$	Induced emf per phase, its estimate and estimation error
ζ, η	Mis-matched disturbance and measurement noise
r_{ph}, $\hat{r}_{ph}$, $\tilde{r}_{ph}$	Phase resistance, its estimate and estimation error
l_{ph}, $\hat{l}_{ph}$, $\tilde{l}_{ph}$	Phase inductance, its estimate and estimation error
θ_m, N_r	Mechanical rotor position and number of rotor poles
θ_e, ω_e	Electrical rotor position and speed
V_{dc}, $\hat{V}_{dc}$	DC-link voltage and its measurement
λ	Pseudo integration variable
ω_{bw}	Closed loop bandwidth
e_i, e_p	Current tracking and parameter estimation errors
$\mathscr{G}_{pp}$	Controller gain obtained via pole placement
K_p, K_i	Proportional and integral gains
W_{pre}, W_{post}	Pre and post filters/compensators
H_p, H_c	Prediction and control horizons
A, B, x, u	State transition matrix, Input matrix, state and control input of a strictly linear system
e_{H_c}, u_{H_c}	Tracking error and control input
J, V	Quadratic cost and value functions
Q, R	Quadratic performance indices for control accuracy and effort respectively
P, $\mathscr{K}$	Value matrix and control gain
ϕ	Input vector
p, $\hat{p}$, $\tilde{p}$	Parameter vector, its estimation and error
σ, γ	Sliding surface and closed-loop pole
υ, ρ	Order of sliding mode and discontinuous

The associate editor coordinating the review of this manuscript and approving it for publication was Christopher H. T. Lee.

$\mathscr{V}$	Lyapunov candidate energy function
Γ	Parameter adaptation gradient
$\|\cdot\|, \|\cdot\|_\infty$	Euclidean and supremum norms

I. INTRODUCTION

On account of its structural robustness, low-cost construction [1] along with the recent development in power converter technology [2], the 'Switched Reluctance Machine' (SRM) drive is becoming a popular choice for increasingly wider array of applications [3]. Especially those involving harsh operating conditions such as, aircraft power generation [4], [5], gas turbine starter/generators [6] and mining [7] have seen successful utilisation of the aforementioned advantages.

Proliferation of SRM drives in industrial applications however, has also aggravated a need for addressing the well known performance issues: the high torque ripple and radial vibrations [1], [8]. Consequently, a wide range of solutions have been explored and rich literature is available covering this subject. These solutions can be broadly classified as, current profiling: offline [9], [10] and online [11], [12], direct torque control(DTC) [13]–[15], and predictive: quadratic regulation [16], [17] and finite control set [18], [19]. Among these solutions, except DTC and finite control set model predictive control, the remaining control techniques are suitable for fixed switching frequency application.

The most prominent advantage of fixed switching frequency operation as opposed to the variable one appears in terms of thermal management, mainly due to uniform distribution of power loss over an electrical cycle. This phenomenon also prevents premature aging of the power electronic devices and allows reliable operation with relatively less exhaustive cooling efforts. In addition, the electromagnetic interference management for fixed switching frequency operation is simpler as compared to its variable switching frequency counterpart [20]. Considering these benefits, there has been a great interest in exploration of fixed switching frequency-based control techniques.

A good estimate of the model dynamics and corresponding disturbances is essential while implementing a fixed switching frequency based control. By principle, the electromagnetic model of SRM is a highly nonlinear dynamical system. The nonlinear variation in the inductance profile over conduction period results into nonlinear flux linkage, torque, radial force, and induced EMF characteristics. Consequently, the optimised phase current profiles developed to achieve one or more of the objectives: torque ripple, RMS phase current and radial force reduction etc. also exhibit highly nonlinear waveforms as functions of rotor electrical position. Thus, demanding fast dynamic response and disturbance rejection from the current controller.

In summary, the problem of achieving optimal performance from SRM drives while maintaining fixed switching frequency of the power converter consists of two parts viz, identification of optimum phase current profile and its tracking. As depicted in Fig.1, closed-loop control of an SRM drive consists of a mechanism for identification of optimum phase current reference as a function of reference torque and rotor position feedback followed by a control law appropriate for fixed switching frequency implementation. The scope of this paper is limited to the latter.

In literature, the developments pertaining to performance enhancement of an SRM drive have been recurrently reviewed. Due to their prominence, the advances in torque control, radial force reduction and efficiency enhancement have received considerable attention in relation to the current control problem. A critical review of the efficiency and accuracy of the optimisation algorithms used for generation of reference phase current profile is provided in [21] while [22] extends this analysis by including conduction angle control. An impressive exposition on optimisation of the torque sharing functions is presented in [23], while [24] and [25] have provided a classification of torque control technologies and their operating principles, where the latter also includes a detailed simulation study.

A limited analysis of the current controllers in terms of digital micro-controller capacity is presented in [26] while [27] have briefly investigated fixed switching frequency PWM control.

A greater analytical depth for current control problem is provided in [28] with emphasis on operating principles of various control techniques whereas [29] and [30] compared the controller performances with detailed simulation studies.

In essence, the literature focusing on the review of fixed switching frequency current control of SRM drives encapsulates the operating principles of the controllers and limited performance evaluation. The interaction of these control laws with the unique non-linear character of the SRM has not received sufficient analytical treatment. The consequences of variation in the dynamic response due to change in operating conditions and corresponding controller response under fixed sampling frequency is a critical aspect which needs a through analysis to quantify and predict the phase current dynamics for different operating conditions as well as to enable the identification the possible avenues for further enhancement in the control performance.

In the light of the above discussion, this paper presents a comprehensive analytical study of the control techniques suitable for fixed switching frequency current control of the SRM drives. The widely implemented current control techniques are identified and classified based on their principles of operation and implementation framework. The paper also presents a critical evaluation of the implementation process of each control technique and provides a theatrical analysis justifying the control performance. On the account of the distinctive electromagnetic characteristics of SRM and from the control hardware perspective, a set of evaluation criterion is developed and used for analysis of each control technique to maintain a uniformity for the purpose of comparison.

The organisation of the rest of the paper is as following. A detailed description of the main challenges faced by an SRM current controller using an electromagnetic model of

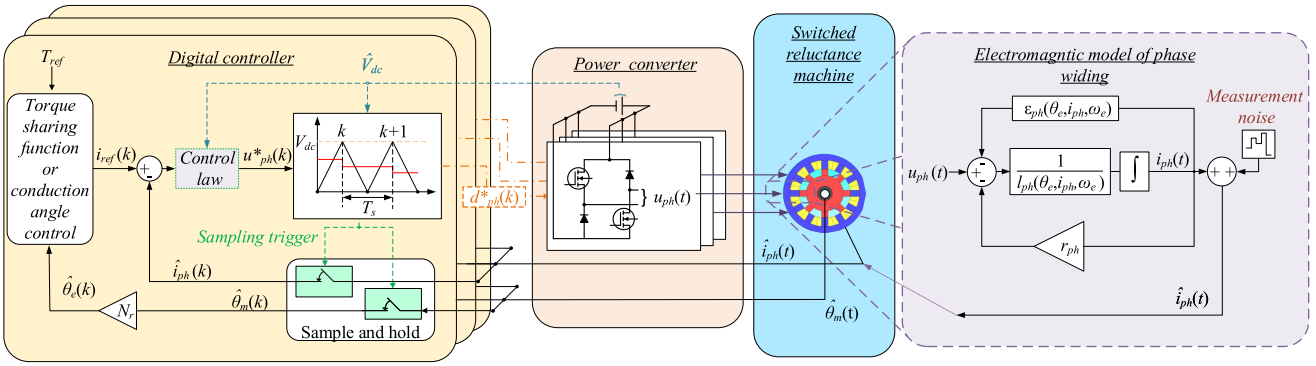

FIGURE 1. Closed-loop control of an SRM drive.

SRM in discrete time domain along with the considerations to the practical implementation aspects, the next Section II provides an evaluation criterion and enlistment of the candidate control techniques. The subsequent Sections III to IX provide analysis of operating principles of each control technique according to the evaluation criteria developed in Section II. The subsequent Section X presents a comparative analysis of the control techniques while the final section XI provides the conclusion and possible avenues for performance enhancement.

II. THE EVALUATION CRITERION AND CANDIDATE CONTROL TECHNIQUES

The current reference profiles optimised for achieving improved performance in SRM drives consist of sharp variations as a function of rotor electrical position [23]. Consequently, these variations get further sped up as mechanical speed increases. Typically for most of the applications, the sampling and switching frequencies are kept constant devoid of the variations in operating speed. Therefore, number of sampling and switching instances per conduction period reduce for higher operating speed.

The matched disturbance in the form of induced EMF also grows proportionally with respect to the speed. Although smooth, the induced EMF characteristics is also highly nonlinear which becomes increasingly challenging to reject due to reduced sampling frequency at higher speeds as the bandwidth of the controller gets severely limited.

The first order representation of electromagnetic characteristics leads to a linear time varying plant, where the time varying nature comes due to the variation in the inductance profile as a function of rotor position. This variation often results into increasingly slower current dynamics in motoring mode and increasingly faster current dynamics in generating mode. Hence, it becomes necessary to adapt the control efforts over conduction period to maintain a consistent dynamic response. Intuitively, this effect also gets exacerbated for higher operating speed.

The above mentioned phenomena are demonstrated ahead with greater clarity by analysing the model dynamics in discrete-time domain.

A. DISCRETE-TIME DOMAIN DYNAMICS OF THE SRM PHASE CURRENT MODEL

As shown in Fig.1, the continuous-time domain current dynamics of SRM can be modelled in the form of a first-order nonlinear dynamical system as,

$$\dot{i}_{ph}(t) = \frac{-\hat{r}_{ph}}{\hat{l}_{ph}(\theta_e, i_{ph})} i_{ph}(t) + \frac{1}{\hat{l}_{ph}(\theta_e, i_{ph})} u^*_{ph}(t) - \frac{1}{\hat{l}_{ph}(\theta_e, i_{ph})} \hat{\epsilon}_{ph}(\theta_e, i_{ph}, \omega_e) - \zeta(t) \quad (1)$$

The mismatched disturbance $\zeta(t)$ in (1) mainly consists of power converter non-linearities, parameter information error, and current measurement noise. The former acts as a discriminant between the voltage commanded by the controller and the phase terminal voltage. Due to the unidirectional nature of the phase current in SRM, the disturbance due to the power converter non-linearities appears as a constant voltage drop [31] and pose no adverse effect on the controller dynamic response. Considering this, the effect of inverter generated disturbance is in not considered in the analysis in the rest of the paper. Accordingly, the controller output voltage is treated to be same as the phase voltage $\left(u^*_{ph}(t) \approx u_{ph}(t)\right)$ and the dynamics of the mismatched disturbance appears only as a lumped sum of the disturbances due to errors in the knowledge of parameters and induced EMF as well as the measurement noise.

If the errors in inductance, resistance and induced EMF profile are defined as: $\tilde{l}_{ph} = l_{ph}(\theta_e, i_{ph}) - \hat{l}_{ph}(\theta_e, i_{ph})$, $\tilde{r}_{ph} = r_{ph} - \hat{r}_{ph}$ and $\tilde{\epsilon}_{ph} = \epsilon_{ph}(\theta_e, i_{ph}) - \hat{\epsilon}_{ph}(\theta_e, i_{ph})$ respectively, the unmodelled dynamics can be expressed as,

$$\zeta(t) = \left[\tilde{r}_{ph} - \hat{r}_{ph}\left(\frac{\tilde{l}_{ph}}{\hat{l}_{ph}(\theta_e, i_{ph})}\right)\right] \frac{i_{ph}}{l_{ph}(\theta_e, i_{ph})} + \frac{\tilde{l}_{ph}}{l_{ph}(\theta_e, i_{ph})}(u_{ph}(t) - \hat{\epsilon}_{ph}(\theta_e, i_{ph}) - \frac{\tilde{l}_{ph}}{l_{ph}(\theta_e, i_{ph})}\tilde{\epsilon}_{ph} + \eta \quad (2)$$

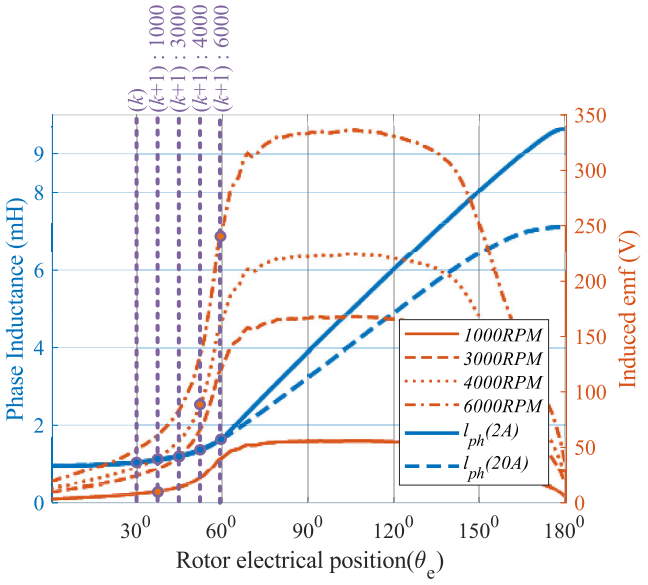

FIGURE 2. Inductance and induced EMF characteristics of a 12-8 SRM for different operating speeds and sampling span at 10kHz frequency.

For a fixed sampling frequency (ω_s), the discrete-time domain counterpart of the current dynamics in (1) becomes:

$$i_{ph}(k+1) = A(k) i_{ph}(k) + B(k)(u_{ph}(k) - \epsilon_{ph}(k)) - \zeta'(k) \quad (3)$$

In (3), the [1 × 1] state transition and input matrices A and B are:

$$A(k) = e^{-\frac{\hat{r}_{ph}}{\hat{l}_{ph}(k)} T_s}$$
$$B(k) = \frac{\hat{r}_{ph}}{\hat{l}_{ph}(k)} \int_{kT_s}^{(k+1)T_s} e^{\left(1 - \frac{\hat{r}_{ph}}{\hat{l}_{ph}(k)}\right)\lambda} d\lambda \quad (4)$$

While $\hat{l}_{ph}(k)$ and $\zeta'(k)$ represent the averaged values of phase inductance and unmodelled dynamics over a sampling period: $kT_s - (k+1)T_s$. In (4), $\hat{l}_{ph}(k)$ is calculated as,

$$\hat{l}_{ph}(k) = \frac{1}{T_s} \int_{kT_s}^{(k+1)T_s} \hat{l}_{ph}(\theta_e, i_{ph}) d\lambda \quad (5)$$

Visual examination of (4) and (5) reveals that the matrices A and B vary as functions of sampling instant, the phase current magnitude and speed. The variation in $\hat{l}_{ph}(k)$ is a function of phase current magnitude as well as rotor position. The effect of magnetic saturation and variation in span of inductance profile being covered per sampling period due to different operating speeds causes the system matrices (4) vary as a function of operating condition. This phenomenon is depicted in Fig.2. The first direct implication of this variation in the system matrices is on the dynamic response consistency. In essence, The increasing inductance profile dictates the need for increasingly large control effort to maintain the desired bandwidth throughout the conduction period and this effect gets further aggravated at higher speed.

B. DISTURBANCES AND UNMODELLED DYNAMICS

The induced emf profile $\hat{\epsilon}_{ph}(\theta_e, i_{ph}, \omega_e)$ and the mismatched disturbance ($\zeta(t)$) appear in discrete-time domain as,

$$\hat{\epsilon}_{ph}(k) = \frac{1}{T_S} \int_{kT_s}^{(k+1)T_s} \hat{\epsilon}_{ph}(\theta_e, i_{ph}, \omega_e) d\lambda$$
$$\zeta'(k) = \frac{1}{T_s} \int_{kT_s}^{(k+1)T_s} \zeta(t) d\lambda \quad (6)$$

As described in (3), $\hat{\epsilon}_{ph}(k)$ appears through the same channel as the input. Therefore, its effect is considered as 'matched'. On the other hand the mismatched disturbance $\zeta(t)$ is not entirely known. However, its nature can be considered smooth and predictable as (2). As depicted in the Fig.2, the magnitude of $\hat{\epsilon}_{ph}(k)$ grows as a function of speed, whereas the magnitude of $\zeta(t)$ depends entirely upon the modelling errors and measurement noise. Both of these factors pose detrimental effect on control performance and demand effective compensation.

C. FREQUENCY WARPING EFFECT AND NEAR BASE SPEED PERFORMANCE

The controller synthesis in continuous-time domain is often approximated for digital implementation by a rule of thumb: $\omega_s \geq 5(\omega_e)$. This approximation helps in identification of maximum controllable electrical speed [32]. This effect grows gradually as the operating speed increases. Therefore, it is essential to verify the consistency in control performance near base speed.

In literature, a myriad of methods is proposed to tackle the above challenges. These methods can be broadly classified as, model-based and observer-based. The model-based systems make use of the knowledge of machine dynamics in the form of phase inductance or flux linkage profile and induced EMF profile, stored in the microprocessor memory. On the other hand, the observer-based systems rely on online identification of the machine dynamics. The main advantage of the model-based systems is the immunity towards noise which allows calculation of numerical derivatives and enables feed-forward compensation of disturbances. However, the discrepancies in the model information and large memory requirement are the main drawbacks of the model-based systems.

The observer-based systems, are more robust to the plant variation. Thanks to their ability to identify changes in the model characteristics online, they can also be used to improve fault tolerance. Consequently, these systems do not need large microprocessor memory. However, online identification process often involve more computational efforts as compared to model-based systems. Also, the identifiablity of the plant cannot be ensured in all the operating conditions and the estimation quality is heavily affected by the noise content in the measurement.

In the view of above discussion, seven criteria are established as shown in Table 1. The order of appearance of each criterion is determined according to the priority: dynamic

TABLE 1. Evaluation criteria for control performance assessment.

No.	Criterion	Category
1	Compensation of inductance variation over conduction period	dynamic response consistency
2	Induced EMF decoupling	Matched disturbance rejection
3	compensation of un-modelled dynamics	Robustness towards mismatched disturbance
4	Frequency warping effect	Performance at high speed
5	Memory utilization	Processor requirements
6	Computational burden	

response consistency, robustness towards disturbances and parameter variation and processing requirements.

TABLE 2. Candidate control techniques under review.

Category	Controller	Application framework
Linear	PI	Fixed gain and dynamic gain scheduling
	H_2/H_∞	Fixed and variable structure
	Linear Quadratic Regulator and Linear Quadratic Gaussian	Model predictive control
	Dead beat	
Non-Linear	Feedback linearizing control	
	Sliding mode	Conventional
		Integral compensation
		Higher order (>2)
	Adaptive	Stability based
		Passivity based

Table 2 provides the classification of the widely implemented control techniques from literature along with their corresponding implementation strategies, specific to the current control of an SRM drive. The purpose of this paper is to provide a sufficiently thorough theoretical analysis of the unique dynamic response of the SRM drive presented earlier in this section, when subjected to the distinct operating principle of each control technique. Although this list is not exhaustive, the control techniques covering in the scope of this paper mainly differ on account of their governing principles and often serve as foundation for advanced versions.

Accordingly, almost all the approaches proposed for fixed switching frequency current control in the literature involve modifications in terms of plant modelling and/or involve combination of one or more control techniques enlisted in Table 2 to achieve improved performance for a specific application.

III. FEEDBACK LINEARIZING CONTROL

The precursor of most of the SRM control technologies can be traced back up to the work by Spong *et al*. [33], [34] addressing the instantaneous torque control of SRM with the help of torque sharing functions and using feedback linearizing (FL) control.

The SRM flux linkage characteristic is a nonlinear function of phase current as well as rotor electrical position. In FL control, linearization is achieved using the knowledge of flux linkage gradient in both current and rotor position. For this purpose, a Fourier series based model is proposed in [34]. According to this model, the phase flux linkage characteristic is represented as,

$$\psi_{ph}(i_{ph},\theta_e) = \psi_s\left[1 - e^{-i_{ph}f_{ph}(\theta_e)}\right] \tag{7}$$

In (7), the nonlinear relation between the phase flux linkage and rotor electrical position is modelled using a strictly positive Fourier series function: $f_{ph}(\theta_e)$ and saturation due to current is modelled by the combination of saturated value of phase flux linkage: ψ_s and an exponential function.

The nonlinear model presented in (7), is continuously differentiable in i_{ph} and θ_e. Thus the phase current dynamics can be readily calculated by taking the partial derivatives of (7) with respect to phase current, $\left(\frac{\partial\psi_{ph}}{\partial i_{ph}}\right)$ as well as the rotor electrical position: $\left(\frac{\partial\psi_{ph}}{\partial\theta_e}\right)$ and stored in microprocessor memory. These functions are utilised to model the phase current dynamics as,

$$\frac{di_{ph}(t)}{dt} = -\left(\frac{\partial\psi_{ph}}{\partial i_{ph}}\right)^{-1}\left[r_{ph}i_{ph}(t) + \frac{\partial\psi_{ph}}{\partial\theta_e}\omega_e\right] + \left(\frac{\partial\psi_{ph}}{\partial i_{ph}}\right)^{-1}u_{ph}(t) \tag{8}$$

Continuous differentiability of $\left(\frac{\partial\psi_{ph}}{\partial i_{ph}}\right)$ and $\left(\frac{\partial\psi_{ph}}{\partial\theta_e}\right)$ functions also ensures the existence of 'diffeomorphism' which enables stable feedback linearization [35]. However, this principle also imposes following constraint:

$$\frac{\partial\psi_{pm}}{\partial i_{ph}} > 0 \tag{9}$$

Intuitively, from (8), a state-feedback linearization can be achieved as [34]:

$$u_{ph}(t) = r_{ph}i_{ph}(t) + \frac{\partial\psi_{ph}}{\partial\theta_e}\omega_e + \frac{\partial\psi_{ph}}{\partial i_{ph}}v_{ph}(t) \tag{10}$$

The linearization achieved using (10) transforms (7) into a linear system. Thus, a constant gain controller is sufficient to achieve necessary dynamic response. The control law $v_{ph}(t)$ in (10) can be obtained via simple pole placement design:

$$v_{ph}(t) = \mathscr{G}_{pp}e_i(t) \tag{11}$$

The overall FL current control scheme is shown in Fig.3. Evidently from (10), The control performance of FL control depends heavily upon the accuracy of the linearizing functions, $\left(\frac{\partial\psi_{ph}}{\partial i_{ph}}\right)$ and $\left(\frac{\partial\psi_{ph}}{\partial\theta_e}\right)$. It is important to note here that, the condition in (9) becomes much more stricter due to finite sampling frequency and DC link voltage limit and a minimum safe value of $\left(\frac{\partial\psi_{ph}}{\partial i_{ph}}\right)$ should be identified experimentally.

Due to the parametric nature of (7), the errors in parameter information leads to deterioration in control law, (10). To address this issue, online adaptation is proposed in [36], [37] and [38]. In [37] the authors proved that for use of nonlinear model in feedback linearization control, the number

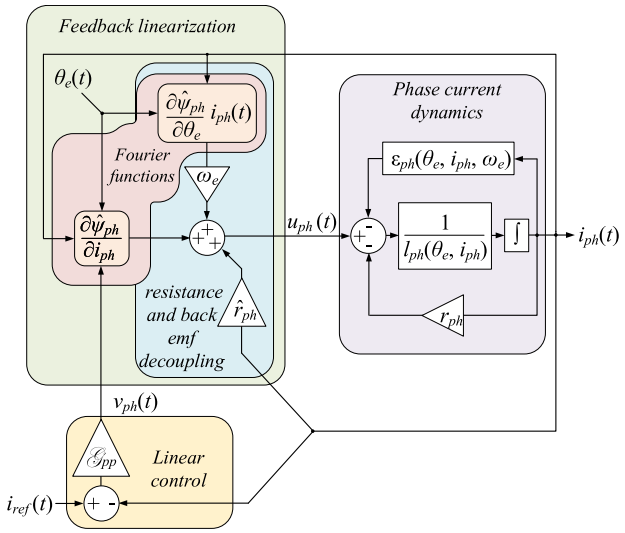

FIGURE 3. Feedback linearizing control.

of parameters to be identified becomes unrealistically high which eventually limits the utility of this method for practical applications.

To reduce the number of parameter, [39] proposed a linear model with reduced number of parameters. However, this provision hampers the control performance for heavy load conditions.

Based on this discussion, the complete performance evaluation of the FL control is presented in the Table 3.

IV. FIXED AND DYNAMIC GAIN SCHEDULING PI CONTROLLER

The use of PI controllers for current control of switched reluctance machines with fixed gains [40]–[42] and [43]–[45] with dynamic gain scheduling are some of the main contributions in this area. Several other contributions also include, fuzzy PI controllers [46], [47] and artificial neural network [48].

The dynamic performance required by the industrial drives cannot be achieved by the linear control techniques such as PI or PID with fixed gains over whole conduction period [36]. A study of fixed PI controller design by Ahmad and Narayanan [49] presents design of linear controllers in four operating conditions: aligned ($\theta_e = 0$ radians) and unaligned ($\theta_e = \pi$ radians) for saturated and unsaturated conditions. It is concluded that the controller design for fully saturated unaligned condition is the best choice to obtain stable performance in all the remaining operating conditions. However, due to fixed nature of controller gain, the consistency in the dynamic response cannot be ensured.

Intuitively, if sufficiently accurate feed-forward decoupling of induced EMF is possible, an analytical equation for inductance profile as a function of current and rotor position can be used to adopt proportional and integral gains. Under this approach, Shulz and Rahman [44] proposed a pole cancellation process neglecting the resistance drop. Therefore,

TABLE 3. Control performance evaluation of FL control.

Criteria	Mechanism
inductance variation	Fourier function: $\left(\frac{\partial\psi_{ph}}{\partial i_{ph}}\right)$
Induced EMF decoupling	Fourier function: $\left(\frac{\partial\psi_{ph}}{\partial\theta_e}\right)\omega_e$
Compensation of parameter variation	Adaptive estimation
Frequency warping effect	Compensation not possible
Memory requirement	Moderate size to store the coefficients of the Fourier series
Computational burden	Very large due to 2-D Fourier series calculations and matrix computation in adaptive estimation

the phase current dynamics reduce to the following form:

$$\frac{di_{ph}(t)}{dt} = \frac{u_{ph}(t)}{l_{ph}(\theta_e, i_{ph})} \tag{12}$$

It is worth noting here that (12) is a small signal representation appearing as a consequence of local linearization. In [43], resistance is also included in the gain adaptation process. Under this approach, the integral gain remains fixed at $r_{ph}\omega_{bw}$ and the proportional gain follows the function:$l_{ph}(\theta_e, i_{ph})\omega_{bw}$.

Similar to [43], Hannoun and Hilairet [45] proposed dynamic adaption in PI gains to maintain a consistently linear 2^{nd} order dynamic response. This approach is more insightful and provides greater flexibility in terms of dynamic performance shaping.

The utility of 'gain scheduling' discussed above, can be demonstrated by analysing the current error dynamics under PI control law:

$$\dot{e}_i(t) + \frac{K_p}{l_{ph}(\theta_e, i_{ph})} e_i(t) + \frac{K_i}{l_{ph}(\theta_e, i_{ph})} \int_0^t e_i(t)dt = 0 \tag{13}$$

For the sake of simplicity, the effect of $\zeta(t)$ is excluded from (13) and the variation in current reference profile is considered slow in comparison with phase current. ($\dot{i_{ph}}(t) \gg \dot{i_{ref}}(t)$). Thus, a linear 2^{nd} order convergence of in the error dynamics at desired bandwidth: ω_{bw} can be achieved with the following gain scheduling scheme [45]:

$$\begin{aligned} K_p &= 2\omega_n l_{ph}(\theta_e, i_{ph}) \\ K_i &= \omega_n^2 l_{ph}(\theta_e, i_{ph}) \end{aligned} \tag{14}$$

With this provision, a consistent error convergence is ensured irrespective of the rotor position as,

$$e_i(t) = e_i(0)(1 + \omega_{bw}t)e^{-\omega_{bw}t} \tag{15}$$

The parameter information necessary to realise PI control law using (14), is stored in the microprocessor memory in the form of 2-dimensional (2-D) Lookup Tables(LUTs) with breakpoints in rotor position and phase current as shown in Fig. 4. Under practical conditions, the parametric error

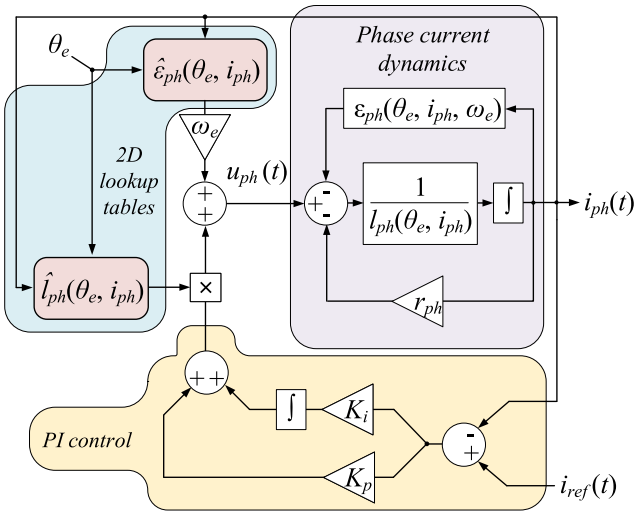

FIGURE 4. PI control with dynamic gain scheduling.

appearing due to errors in current and position measurement and modelling imperfections, the unmodelled dynamics ((2)) appear in the form of damped oscillations due to asymptotic nature of disturbance compensation by PI controller. By principle, the effectiveness of compensation provided by PI controller is inversely proportional to oscillation frequency of $\zeta(t)$. Thus, at higher speed, the compensation also reduces significantly which eventually threaten the control loop stability. In such case, an artificial damping effect is generated by virtually dissipating the control energy [50].

Unlike FL control, PI control is developed using 'Jacobi linearization' which employs local linearization of the machine dynamics instead of a transform. A detailed account on this difference can be found in [51]. The inductance lookup table used for dynamic adaptation in the controller gain represents locally linearized model of phase winding. This approach is effective when the difference in the model information for successive sampling instances is sufficiently small. As the speed increases, increasingly large variations in the inductance profile causes deterioration in the control performance. This phenomenon is essentially the origin of the frequency warping effect discussed in Section II.

The above discussion is summarised under control performance evaluation criterion in Table 4.

V. H_2/H_∞ CONTROL

One of the most reliable feedback optimisation methods, H_2/H_∞ synthesis is classified as a robust control technique. This approach involves identification of an optimum control structure which provides desired closed-loop characteristics over a wide frequency range. One of the main advantages of H_∞ control lies in its suitability for multi-input, multi-output systems with considerable cross-coupling. However, for a fixed structure application, the system order becomes impractically large and approximate reduction becomes necessary which often comes at the expense of performance

TABLE 4. Control performance evaluation of PI control.

Criteria	Mechanism
inductance variation	Dynamic gain scheduling Using inductance LUT
Induced EMF decoupling	Feed-forward compensation using induced EMF LUT
compensation of parameter variation	Controller effort aided by active damping
Frequency warping effect	significant due to Jacobi linearization
Memory requirement	large memory requirement for the storage of inductance and induced EMF LUTs
Commputational burden	Moderate, mainly due to interpolation over 2-D LUTs

degradation. Moreover, sufficient care should be taken for application in the sampled data systems with signification sampling delays. In switched reluctance machines, the H_2/H_∞ control techniques have found application for speed control [52], [53] and specifically for current control, [54], [55].

Two main approaches for H_2/H_∞ controller design are: fixed structure synthesis and normalisation of co-prime factorisation [56]. Both of these approaches involve normed minimisation of the closed-loop transfer function. In particular, for H_∞ design, a supremum norm minimisation is performed:

$$\min_{W_{pre}(s),K_h,W_{post}(s)} \left\| \frac{G_p(s)}{1 + G_p(s)W_{pre}(s)K_hW_{post}(s)} \right\|_\infty \quad (16)$$

whereas, an H_2 design is obtained via minimisation of a Euclidean norm:

$$\min_{W_{pre}(s),K_h,W_{post}(s)} \left\| \frac{G_p(s)}{1 + G_p(s)W_{pre}(s)K_hW_{post}(s)} \right\| \quad (17)$$

In (16) and (17), $G_p(s)$ represents the open-loop transfer function of SRM phase winding and K_h is the controller gain. Similar to the FL and PI control designs, gain adaptation as a function of the inductance profile and induced EMF decoupling can be employed to simplify the design process [54], [55]. The resultant control realisation thus obtained, is shown in Fig.5. It is perceivable from (16) and (17) that H_∞ is more conservative approach as compared to H_2 and should be preferred under noisy measurement conditions.

In the above discussed structure of H_2/H_∞ control, the value of K_h is defined to maintaining desired bandwidth while the post filter W_{pre} is used as a compensator to improve stability margins. As discussed earlier, the switched reluctance machine is a nonlinear plant hence, K_h is varied as a function of rotor position while W_{post} resembles a PI controller.

All the approaches in the literature present continuous-time domain designs. In addition to the bandwidth limitation arising due to the post filter, the tracking capability of H_2/H_∞ controllers deteriorate as the operating speed increases and similar to the PI control, the limitations arising due to frequency warping effect are also persistent.

TABLE 5. Performance evaluation of H_2/H_∞ Control.

Criteria	Mechanism
inductance variation	Adaptation in K_h using inductance LUT
Induced EMF decoupling	Feed-forward compensation using induced EMF LUT
compensation for unmodelled dynamics	Lead compensation using W_{pre}
Frequency warping effect	significant due to Jacobi linearization
Memory requirement	Large memory is required for the storage of 2-D inductance and Induced EMF LUTs
Commputational burden	Moderate, mainly due to the interpolation over 2D LUTs

Although the H_2/H_∞ synthesis is readily applicable for multi-input multi-output systems, for SRM current control, it is sufficient to consider independent Single-Input Single-Output (SISO) systems per phase, unless there is a significant effect of mutual coupling.

In a nutshell, the H_∞ control synthesis provides additional flexibility over PI control design in terms dynamic response shaping and disturbance rejection. Especially under the effect of phase margin degradation due to aggressive control effort, the lead compensator or saturation, (W_{pre}) becomes very useful. Moreover, as opposed to PI design alone, the compensation of the unmodelled dynamics described in (2) is far more effective in H_2/H_∞ control.

A summary of the performance analysis of H_2/H_∞ control discussed in this section is presented in Table 5.

VI. LINEAR QUADRATIC REGULATOR (LQR) AND LINEAR QUADRATIC GAUSSIAN (LQG)

The LQR design is considered as a breakaway from the conventional stability margin-based designs discussed in the previous sections. Under this approach, an optimal state estimator is often employed to achieve greater noise immunity, resulting into an LQG design.

A typical LQR/LQG design involves identification of an optimum sequence of the control input over a desired number of future sampling instances, known as control horizon (H_c). For a strictly linear SISO system, a Controlled Auto-Regressive Integrated Moving-Average (CARIMA) model is employed to identify the state dynamics for a span of future sampling instances know as prediction horizon ($H_p > H_c$):

$$\begin{bmatrix} x(k+1) \\ \vdots \\ x(k+H_c) \\ \vdots \\ x(k+H_p) \end{bmatrix} = \begin{bmatrix} B & \cdots & 0 & \cdots & 0 \\ \vdots & \ddots & \vdots & \ddots & \vdots \\ A^{H_c-1}B & \cdots & 0 & \cdots & 0 \\ \vdots & \ddots & \vdots & \ddots & \vdots \\ A^{H_p-1}B & \cdots & A^{H_c-1}B & \cdots & B \end{bmatrix} \begin{bmatrix} u(k) \\ \vdots \\ u(k+H_c-1) \\ \vdots \\ u(k+H_p-1) \end{bmatrix} + \begin{bmatrix} A \\ \vdots \\ A^{H_c} \\ \vdots \\ A^{H_p} \end{bmatrix} x(k) \tag{18}$$

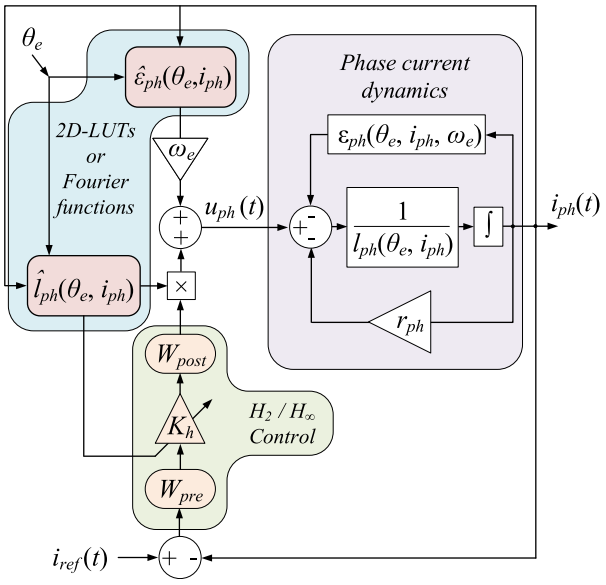

FIGURE 5. H_2/H_∞ control.

While, the cost function is defined on the basis of a trade-off between the control accuracy and the effort as:

$$J = \frac{1}{2}\left[e_{H_c}^T Q e_{H_c} + u_{H_C}^T R u_{H_c}\right] \tag{19}$$

In (18), the magnitudes of the $[H_c \times H_c]$ positive symmetric matrices Q and R act as weighing functions. For Constant A and B matrices, the entire control sequence can be identified by obtaining an offline solution for the 'Algebraic Riccati Equation'(ARE) corresponding to the model (18) and cost function J. As described in Section II, the switched reluctance machine does not exhibit a linear dynamical behaviour. Hence, the approach presented above, cannot be directly utilised to ensure a reliable tracking performance and a fixed gain structure is sufficient only for the development of a stable sub-optimal controller. In literature, this issue is addressed from the modelling point of view. Except [57], the model information is stored in the form of locally linearized flux-linkage or inductance lookup tables [17], [58] [59]. The main advantage of this approach is that, it ensures the validity of algebraic approximation of the differential Riccati equation [60]. With augmentation of parameter estimation mechanism the complete LQR/LQG control loop can be represented as shown in the Fig.6.

In optimal control theory, the SRM current control design is classified as a servo control problem [61]. Under this approach, for a given control horizon of H_c, the quadratic performance index at a sampling instant k is defined as,

$$V(k) = \sum_{i=k}^{k+H_c} (e_i(i)^2 Q + u_{ph}^2(i) R) \tag{20}$$

Due to its simple structure, almost all the LTV approaches presented in literature involve a flux linkage based model as opposed to the inductance based model. The relation between

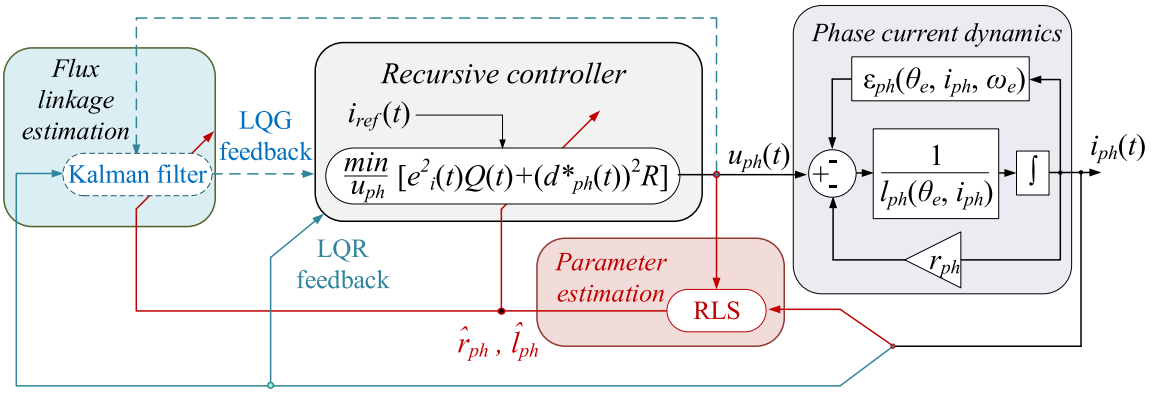

FIGURE 6. LQR/LQG control.

these models can be described as,

$$\psi_{ph}(t) = i_{ph}(t)l_{ph}(t)$$
$$\Rightarrow \frac{d\psi_{ph}(t)}{dt} = l_{ph}(t)\frac{di_{ph}(t)}{dt} + \epsilon_{ph}(t) \quad (21)$$

By substitution of (21) in (1), a 'Linear Time Varying'(LTV) state space representation of the tracking control problem is obtained as,

$$X_\psi(k+1) = A(k)X_\psi(k) + Bu_{ph}(k) \quad (22)$$

where,

$$A(k) = \begin{bmatrix} \left(1 - \frac{\hat{r}_{ph}}{\hat{l}_{ph}(k)}\right) & 0 \\ 0 & F(k) \end{bmatrix}$$

is a state transition matrix and $B = \begin{bmatrix} T_s & 0 \end{bmatrix}^T$ is an input matrix. The reference profile model, $i_{ref}(k+1) = F(k)i_{ref}(k) + i_c$ is an LTV system whose dynamics are well known. Consequently, the new quadratic performance index becomes [62]:

$$\mathscr{V}(k) = \sum_{i=k}^{H_c} \left[X^T_\psi(k)Q'(k)X_\psi(k) + u^2_{ph}(k)R\right] \quad (23)$$

where, the new performance index responsible for current regulation accuracy is a time varying function defined as,

$$Q'(k) = \begin{bmatrix} \frac{Q}{l^2(k)} & \frac{-Q}{l(k)} \\ \frac{-Q}{l(k)} & Q \end{bmatrix} \quad (24)$$

This provision stipulates necessary adaptation in the current controller gain to maintain a constant bandwidth over entire conduction period. In [58], [61] and [17], the optimisation variable Q for locally linearized model is stored in the form of an LUT to be utilised for online computation of optimum controller gain. Noticeably, this scheme assumes availability of accurate parameter information. Thus, optimum trajectory can be split into its constituents, each spanning over a sampling period [63]:

$$X^T_\psi(k)P(k)X_\psi(k) = X^T_\psi(k)Q'(k)X(\psi)(k) + u^2_{ph}(k)R$$
$$+X^T_\psi(k+1)P(k)X_\psi(k+1) \quad (25)$$

where, $P(k)$ is a positive symmetric matrix to be identified in each sampling instant, from a 'Hamiltonian' function given below.

$$\begin{aligned}&\mathscr{H}(k)\\ &= X^T_\psi(k)Q'(k)X_\psi(k) - X^T_\psi(k)P(k)X_\psi(k)\\ &\quad +X^T_\psi(k)\Big[\mathscr{H}(k)^T R\mathscr{H}(k) + A(k)^T P(k)A(k)\Big]X_\psi(k)\\ &\quad +X^T_\psi(k)\Big[A(k)^T P(k)B\mathscr{H}(k) + \mathscr{H}(k)^T B^T P(k)A(k)\\ &\quad +\mathscr{H}(k)^T B^T P(k)B\mathscr{H}(k)\Big]X_\psi(k) \end{aligned} \quad (26)$$

The convexity of (26) is ensured by considering linear nature of the machine model over a sampling period. Therefore, the optimum control voltage for a sampling instant, k can be defined as $u_{ph}(k) = \mathscr{K}(k)X_\psi(k)$ where, $\mathscr{K}(k)$ is constant over a sampling period. The solution of this Hamiltonian results into $u_{ph}(k)$ as a function of $\psi_{ph}(k)$ feedback and $i_{ref}(k+1)$ feed-forward terms [64].

$$u_{ph}(k) = \frac{P_{11}(k)\left(1 - \frac{\hat{r}}{\hat{l}(k)}\right)T_s}{(R + T_s^2)}\psi_{ph}(k)$$
$$+\frac{P_{12}(k)T_s}{(R+T_s^2)}i_{ref}(k+1) \quad (27)$$

For some systems, the dc link voltage is measured with the help of a voltage sensor and inductance and resistance are identified using either least square or adaptive parameter estimation. A least square based estimation algorithm tries to fit a the nonlinear SRM model into a linear LTI system as,

$$\psi_{ph}(k) = \phi^T(k-1)p \quad (28)$$

In SRM however, the parameter vector:

$$p(k) = \begin{bmatrix} \left(1 - \frac{r}{l(k)}\right) & T_s \end{bmatrix}^T$$

is a time varying quantity being modelled using the input vector: $\phi^T(k-1) = [\psi_{ph}(k-1) \quad u_{ph}(k-1)]$. Intuitively, an assumption on insignificant variation in parameters over successive sampling instances is inevitably involved in this process [17]. In the view of time varying nature of the parameters, a 'Recursive Least Square' (RLS) algorithm naturally becomes the best choice thanks to its computational economy and fast response [65]. Assuming sufficiently low noise in current sensing, two sampling instances can be considered sufficient to obtain accurate parameter information. Accordingly, following equation is implemented recursively.

$$\begin{aligned} p(k) &\approx p(k-1) \\ &= \Big[\phi(k-1))(\phi^T(k-1)) + \phi(k-2))(\phi^T(k-2))\Big]^{-1} \\ &\quad \cdot \big[\phi(k-1)\psi_{ph}(k) + \phi(k-2)\psi_{ph}(k-1)\big] \end{aligned} \tag{29}$$

The identified parameters via (29) at a sampling instant are averaged over two preceding instances. Thus incurring a delay of 1.5 samples. This value can be reduced very close to 1 by addition of an exponential forgetting factor [66]. However, it comes at the cost of higher reliance over the latest samples. Considering accurate DC link voltage measurement and its constant nature, the knowledge of second parameter can be considered very well known and its contribution to the overall error being negligibly minimum. The estimated parameters appear as inverse of the inductance. Considering this effect, if the multiplicative uncertainty is defined as, $\delta a(k) = \frac{1}{1+\frac{\tilde{l}(k)}{l(k)}}$, the corresponding deterioration in the control accuracy performance index becomes:

$$\Delta Q'(k) = \begin{bmatrix} \dfrac{(\delta a(k)-1)Q}{l^2(k)} & -\dfrac{(\delta a(k)-1)Q}{l(k)} \\ -\dfrac{(\delta a(k)-1)Q}{l(k)} & 0 \end{bmatrix} \tag{30}$$

Along with the error in the estimated state transition matrix, the error in Hamiltonian becomes:

$$\begin{aligned} \delta\mathscr{H}(k) = {} & x_\psi(k)^T \delta A^T P(k) X_\psi(k) \\ & + X_\psi^T(k)\delta A(k) P(k) B X_\psi(k) \\ & + X_\psi^T(k)^T B^T P(k)\delta A(k) X(k) \end{aligned} \tag{31}$$

The dynamics of (31) are exactly the same as the discrete-time domain counterpart of unmodelled dynamics represented in (2). As the speed increases, the magnitude of $\delta\mathscr{H}(k)$ grows which further deteriorates the control performance.

VII. SLIDING-MODE CONTROL

The proven robustness characteristics of the sliding mode control(SMC) technology have inspired several applications in SRM control. Due to very fast dynamics of the electromagnetic model, the classical discontinuous switching function based sliding mode control alone becomes infeasible for current control application due to limited sampling and switching frequencies. However, PI aided hybrid [67] and integral compensation [68], [69] have been successfully implemented

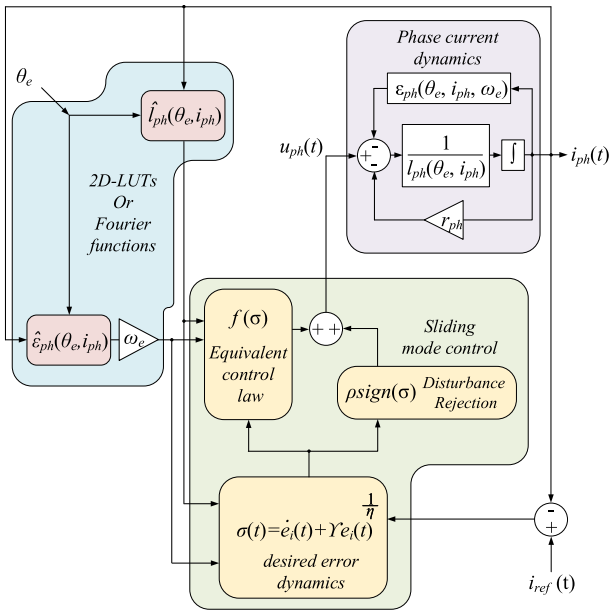

FIGURE 7. Sliding mode control.

TABLE 6. Performance evaluation LQR/LQG control.

Criteria	Mechanism
inductance variation	Scheduling of control accuracy performance index(Q)
Induced EMF decoupling	Estimation of flux linkage dynamics using state estimator (LQG) or inductance information alone (LQR)
compensation of parameter variation	Online estimation of inductance using RLS
Frequency warping effect	Significant due to Jacobi linearized models used in state and parameter estimation
Memory requirement	Moderate, storage of Q function or inductance map is required
Computational burden	Very large due to recursive-nature of the algorithms involved in solving Hamiltonian at each time step

with good tracking performance. The loss of finite time convergence in these methods led to further investigation in higher order sliding-modes such as second order [70], [71] and terminal [72].

The phase current dynamics of all the electrical machines including SRM are classified as relative degree 1 systems since the control voltage term appears as a function of 1^{st} derivative of phase current. Therefore, the desired dynamic response can be defined as:

$$\sigma(t) = \dot{e}_i(t) + \gamma |e_i(t)|^{\frac{1}{\upsilon}} sign(e_i(t)) \tag{32}$$

The parameters γ defines the overall control effort which is analogous to the desired closed-loop pole in classical control terminology, whereas tuning υ helps in optimising control effort near $e_i(t) = 0$. A good engineering judgement prescribes consideration of robustness towards measurement noise while maintaining fast dynamic response while choosing γ and υ. Perhaps the most important aspect of sliding mode control design is the balance between equivalent control and disturbance rejection terms [73]. This principle

can be demonstrated by analysing the control design process described ahead.

With *a priori* knowledge of the reference and phase current dynamics, (1) the optimum control voltage can be obtained by equating the sliding surface, (32) to zero. However, due to presence of $\zeta(t)$, it is not possible to accurately realise optimum $u_{ph}(t)$ which can effectively achieve and maintain $\sigma(t) = 0$. In an ideal sliding mode control design, this issue can is tackled by defining the control input into its known and unknown components: $u_{ph}(t) = u_{1ph}(t) + u_{2ph}(t)$ where $u_{1ph}(t)$ constitutes known part of $\sigma(t)$ dynamics and called as equivalent control law:

$$u_{1ph}(t) = \hat{l}_{ph}(\theta_e, i_{ph})\dot{i_{ref}}(t) + \hat{r}_{ph}i_{ph}(t) + \hat{\epsilon}_{ph}(\theta_e, i_{ph}) - \gamma|e_i(t)|^{\frac{1}{\upsilon}}sign(e_i(t)) \quad (33)$$

The second component of the input voltage: $u_{2ph}(t)$ is designed to compensate for the effect of $\zeta(t)$ and attain $\sigma(t) = 0$ also called as the reaching phase. By minimisation of a candidate Lyapunov energy function: $\mathscr{V}_i(t) = \frac{\sigma^2(t)}{2}$ with respect to $u_{ph}(t)$ and substitution: (33), the disturbance compensation term $u_{2ph}(t)$ is obtained as,

$$u_{2ph}(t) = \rho sign(\sigma(t)) \quad (34)$$

where, the amplitude of the discontinuous switching term (ρ)in (34) is determined considering a conservative bound on unmodelled dynamics and desired rate of descend for $|\sigma(t)| = \alpha(\alpha > 0)$.

$$\rho = \|\zeta(t)\|_\infty + \frac{\alpha}{\sqrt{2}} \quad (35)$$

Fig.7 depicts SRM phase current control using above formulation of sliding-mode control.

An optimum control design demands minimum magnitude of the discontinuous switching while maintaining necessary rate of convergence during reaching phase. This can be achieved by maximising utilisation of a priory model information and reference current dynamics. This principle is very well demonstrated in [68]. However, $\dot{i_{ref}}(t)$ is still considered unknown. This exclusion results into additional increase in magnitude of ρ.

TABLE 7. Performance evaluation of sliding-mode current control.

Criteria	Mechanism
inductance variation	Gain adaptation in equivalent control law using inductance profile
Induced EMF decoupling	Feed-forward decoupling using induced EMF profle
Compensation of unmodelled dynamics	High frequency approximation using discontinuous switching control
Frequency warping effect	Accuracy of equivalent control law reduces at high speed which is compensated by discontinuous switching control
Memory requirement	Induced EMF and inductance profile
Computational burden	Low due to non iterative process. However, calculation of υ^{th} root of current tracking error is expensive

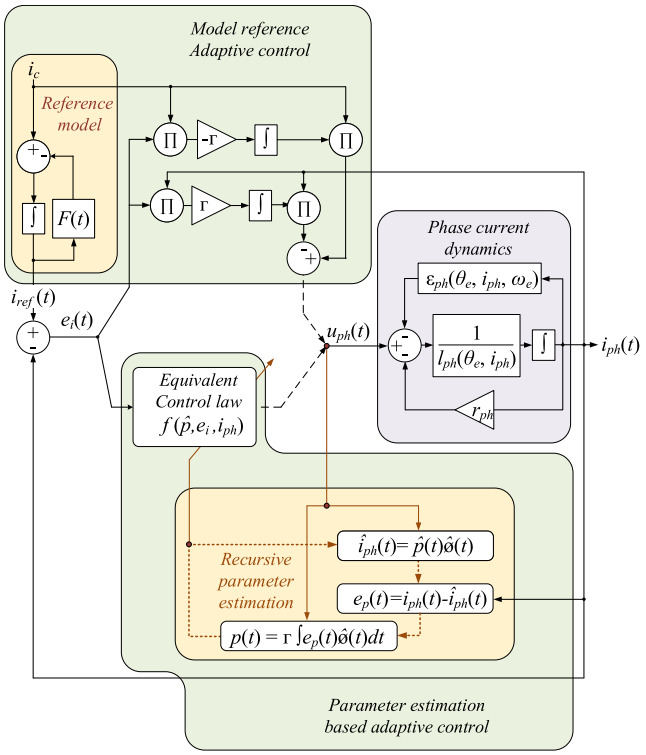

FIGURE 8. Adaptive control.

Based on the this discussion, it becomes clear that the error in parameter information is the primary source of control performance deterioration for the quadratic regulators. Nevertheless, the utility of this control technique has been proved in the literature with good tracking accuracy for reasonable magnitude of switching frequency. Based on the above discussion, the control performance assessment of quadratic regulators is summarised in Table 6. It is also worth noting here that, the designs proposed in the literature and in this section belong to continuous-time domain which stipulates a strict limit on the frequency content of unmodelled dynamics for effective high frequency approximation of $\zeta(t)$ during sliding phase.

The performance evaluation of sliding mode control based on above discussion is summarised in Table 7.

VIII. ADAPTIVE CONTROL

The time varying nature of phase inductance profile in SRM pose a great challenge in terms of adaptive control synthesis for the SRM phase model (1). However, tracking accuracy improvement has been reported by augmenting parameter adaptation mechanism with feedback linearization by Taylor *et al*. [74] and Bortoff [75] while Peng [76] and Szamel [77] employed adaptive parameter estimation in dead-beat control. A more traditional approach of model reference adaptive control(MRAC) is demonstrated in [78].

The adaptive control mechanisms introduced above are performed using stability based designs [79], while the passivity based control realisation can be found in [80] and [81].

Both approaches operate on the principle of energy function shaping. For SRM current control however, the methods proposed in the literature can be classified as model reference based and parameter estimation based. The control implementation using both the approaches is depicted in Fig.8.

The performance of these methods can be evaluated by analysing the control implementation processes for each of these techniques. Under MRAC approach, the control objective is to follow the current reference profile model:

$$\dot{i_{ref}}(t) = F(t)i_{ref}(t) + i_c(t) \tag{36}$$

(36) is a continuous-time equivalent of the reference profile model introduced in Section VI. By treating the induced EMF $\epsilon_{ph}(t)$ as a part of the $[1 \times 1]$ state matrix, following control and adaptation laws can be defined:

$$u_{ph}(t) = \hat{p}(t)\phi(t), \dot{p}(t) = [\,-\Gamma\ \Gamma\,]^T\, e_i(t)\phi(t) \tag{37}$$

where,

$$\hat{p}(t) = [\,\hat{p}_1(t)\ \hat{p}_2(t)\,]^T$$

and

$$\phi(t) = [\,i_c\ -i_{ph}(t)\,]^T\,.$$

The performance of the control action described in (37) can be evaluated by analysing its corresponding class K Lyapunov energy function:

$$\mathscr{V}(k) = \frac{1}{2}\left[e_i^2(t) + \left(p(t) - \hat{p}(t)\right)^T Q\left(p(t) - \hat{p}(t)\right)\right] \tag{38}$$

where, $Q = \Gamma^{-1}I_{[2\times 2]}$ and the parameter vector becomes,

$$p(t) = \left[\,F(t) - \frac{r_{ph}}{l_{ph}(\theta_e, i_{ph})} - \frac{1}{l_{ph}(\theta_e, i_{ph})}\frac{dl_{ph}(\theta_e, i_{ph})}{dt}\ l_{ph}(\theta_e, i_{ph})\,\right]^T$$

On the other hand, for an equivalent control law based realisation, the parameter and input vectors are defined according to (28). Similar to MRAC, a well justified candidate Lyapunov function: $\mathscr{V}(t) = \frac{e_p^2(t)}{2}$ yields following adaptation law:

$$\dot{\hat{p}}(t) = -\frac{\partial \mathscr{V}}{\partial p} = \Gamma e_p(t)\phi(t) \tag{39}$$

In both MRAC as well as equivalent control based formulation, the real parameter vectors are highly non-linear functions of time. Therefore, it is very difficult to perform adaptation in $\hat{p}(t)$ with sufficient accuracy. However, for MRAC, any combination of $\hat{p}(t)$ which results into minimisation of $\mathscr{V}(t)$ in (38) at a reasonable rate is sufficient. Whereas, the conditions on $\hat{p}(t)$ are more stringent for equivalent control law based realisation since it is required to attain the real values of parameters only. This condition also inevitably calls for sufficient 'richness' in the frequency content of the input: $u_{ph}(t)$ [82]. Naturally, it is not possible to satisfy this constraint in every operating condition.

Considering the above discussion, the approach in [78] appears to be more reasonable. However, in equivalent control law based control, the initiation of $\hat{p}(t)$ can be performed in the neighbourhood of the real parameters where the energy function: (28) is convex. A successful demonstration of this concept using a flux linkage LUT is presented in [76]. The overall performance evaluation of adaptive control is presented in Table 8.

TABLE 8. Performance evaluation of adaptive control.

Criteria	Mechanism
inductance variation	Inductance LUT and parameter estimation(for equivalent control law) control parameter adaptive (for MRAC)
Induced EMF decoupling	Incorporation of induced emf dynamics in state matrix
compensation of parameter variation	online estimation
Frequency warping effect	rate of adaptation can be optimised to adjust for faster change in parameters.
Memory requirement	Inductance LUT for equivalent control law
Commputational burden	Moderate due to matrix multiplication involved in the parameter adaptation process

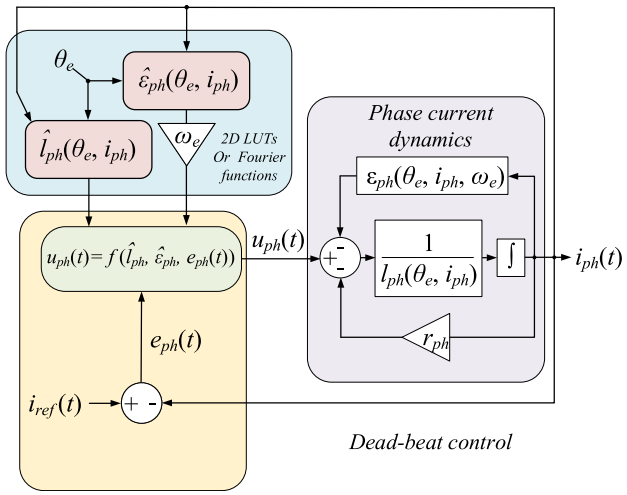

FIGURE 9. Dead-beat control.

IX. DEAD-BEAT CONTROL

Due to their fast dynamic response and, simple structure, the dead-beat controllers have been widely implemented for current control problems. The major contributions include, predictive: [16], [59] predictive with parameter adaptation [76], using iterative learning control [83] and using torque sharing functions [84]. A typical application process using dead-beat control is shown in (9).

Except the asymptotic convergence type techniques, The remaining control techniques mentioned in proceeding sections can produce deadbeat type of performance, such as, the LQR/LQG with $R = 0$, [58], [85] and sliding mode control with manifold $\sigma(t) = \dot{e}_i(t)$. In a nutshell, the deadbeat control determines the optimum control voltage to achieve the desired current reference within a sampling period using the knowledge of the measured current feedback and available model information.

Intuitively, the very large gain of deadbeat controller makes the control loop highly susceptible to the measure-

ment noise. Use of optimal state estimation becomes very promising in this scenario. Except large magnitude of the gain, the behavior of a dead-beat controller is similar to the previously mentioned control techniques and the performance evaluation can be considered based on the application framework.

X. COMPARATIVE ANALYSIS OF CONTROL TECHNIQUES

The analysis of the candidate control techniques presented in sections III-IX illustrates their operating principles in the context of the performance criterion enlisted in Table 1 and provides corresponding elucidations. On account of these discussions, this section presents a comparative analysis of these control techniques adhering to the same evaluation criterion.

As shown in Fig.10, the control techniques with identical design processes and implementation frameworks are grouped on a single spider-plot for comparison. It is worth noting here that the immunity towards measurement noise is not expressed exclusively as a comparison criterion in this section. However, its effect is considered over the attributes: dynamic response consistency, induced EMF decoupling and robustness towards parameter variation. The ratio, switching to electrical frequency: $\frac{\omega_f}{\omega_e}$ essentially expresses the physical implication of the frequency warping effect discussed in Section II. The assessment metric for each comparison criterion is kept the same across all the spider-plots shown in Fig.10 enabling uniformity for the purpose of analysis. Thus, all the control techniques shown in Fig.10(*a-e*) can be analyzed in relation to each other. The rest of this section provides a discussion on the comparative analysis of the control techniques.

Fig.10(*a*) Shows the comparison among the fixed gain PI, and robust control techniques: H_2 and H_∞. Due to fixed nature of its gain, the PI controller is not capable of maintaining a consistency in the dynamic response. Moreover, its ability to counter the disturbance due to back EMF is also inconsistent across the operating conditions. H_2 and H_∞ demonstrate a trade-off between dynamic response consistency and the ability to reject matched (induced EMF) and mismatched disturbances. As discussed in Section V, the conservative nature of H_∞ design also performs better at higher speed owing to its better disturbance reject ability. Due to the relatively low phase margin, the PI controller alone exhibits the performance inferior in compared to H_2 and H_∞ designs. Whereas, due to implementation simplicity, it has the best computational and memory efficiency.

The use of model information allows dynamic adaptation of the PI controller gain as a function of rotor position. FL control also emulates similar adaptation in the closed loop gain with the help of $\frac{\partial \psi_{ph}}{\partial i_{ph}}$ and $\frac{\partial \psi_{ph}}{\partial \theta_e}\omega_e$ functions introduced in Section III.

Thanks to the integral action, the PI controller provides better noise rejection thus improving the dynamic response, induced EMF decoupling and parameter insensitivity. However, the corresponding drop in phase margin reduces its performance at higher speeds than pole placement design based FL control. Highly parametric nature of the Fourier series functions in FL control demands relatively large

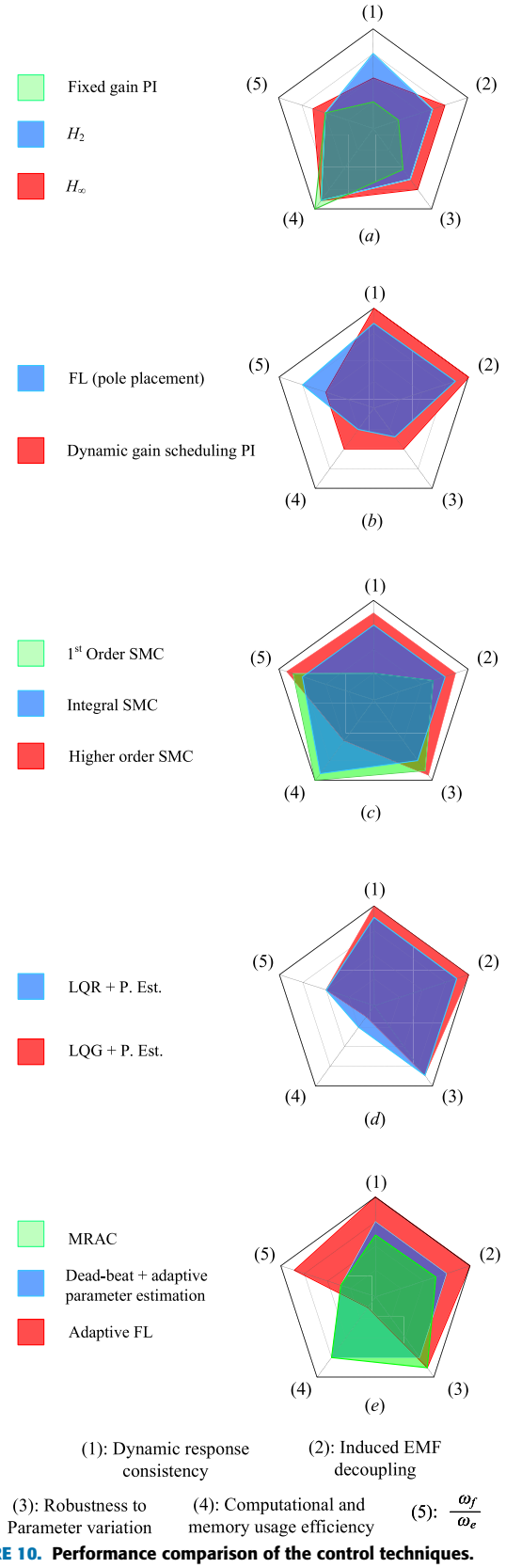

FIGURE 10. Performance comparison of the control techniques.

processing efforts and suffers from performance degradation due to parameter drift.

Sliding mode approach provides the most robust control design among the techniques reviewed in this paper. Due to its discontinuous switching action, the 1^{st} order sliding mode control exhibits inconsistency in the dynamic response as it is not possible to perform a high-frequency approximation of the disturbances in digital applications. The magnitude of the discontinuous switching function is optimal for the worst-case condition only and hence results in chattering about the sliding surface. Consequently, the phase current also suffers large ripple about the reference. On the other hand, SMC with integral compensation attains a good compromise between corrective and disturbance rejection efforts. However, the integral compensation does not allow finite-time convergence, limiting its performance at higher speeds. Elimination of the discontinuous switching while maintaining a finite time convergence can be achieved with the help of higher-order SMC. However, due to the large computational burden imposed by the calculation of fractional powers of the tracking error, all higher-order SMC designs (≥ 2) suffer from low computational efficiency.

Among the optimal control techniques presented in the literature, the linear regulators with augmented parameter estimation mechanisms have demonstrated excellent tracking performance. As detailed in Section VI, both LQR and LQG design approaches discussed in the literature employ 1^{st} order model of phase winding. Due to the time-varying nature of the SRM inductance profile, the parameter estimation mechanism suffers a unit time step delay in estimated parameters resulting in performance degradation at higher speeds. In terms of dynamic response consistency, and disturbance rejection ability, LQG performs better than LQR due to its better noise immunity. On the other hand LQG is more computationally expensive owing to the presence of an optimal state estimator.

As described in Section VIII, due to fast time-varying nature of 1^{st} order models, the adaptive control becomes very challenging. On the other hand, constant parameter based Fourier series models exhibit slow time varying nature, which is more suitable for adaptive estimation. However, large number of parameters adds to the computational burden and memory usage.

XI. CONCLUSION

The paper focuses on the important aspects pertaining to fixed switching frequency current control of SRM. The need for high dynamic response due to fast varying current reference command, compensation of nonlinear induced EMF and inductance variation over a conduction period are considered for evaluation of control technique performance. The frequency warping phenomenon is also considered to predict the performance at high speed.

Due to highly nonlinear electromagnetic characteristics of SRM, use of model information in the form of inductance or flux linkage profile for maintaining consistency in dynamic performance is seen prevalent thorough the literature. Similarly, the highly nonlinear induced EMF is compensated for using an induced EMF lookup table. These techniques, although pragmatic, need large storage in micro controller memory and suffer from model mismatch due to interpolation issues as well as variation in the parameters during regular operation. The latter constitutes unmodelled dynamics, the effect of which is also analysed.

On account of this study, the rest of this section, presents several recommendations for further improvement in the performance of the control techniques discussed in this paper followed by the concluding remarks.

A. RECOMMENDATIONS FOR PERFORMANCE IMPROVEMENT

1) NON-LINEAR MODELLING

The first order Jacobi linearized model with inductance lookup table based scheduling rely on the assumption that the Euler's approximation of discretization remains fairly accurate. As discussed in Section II, the validity of this assumption gradually reduces as a function of speed. This phenomenon is one of the reasons for performance deterioration at high speed. Thus, replacing the constant value of the inductance over a sampling period with a function can potentially improve the performance.

As a consequence of the non-liner modelling, the formulation of LQR/LQG problem becomes more complex and more efficient algorithms for solving the Hamiltonian function (26) deserve further exploration.

For MRAC realisation, the non-linear modelling helps in transformation of SRM model from a 'fast LTV' to a 'Slowly Time Varying(TV)' plant [86]. Although the slowly TV plant has more parameters, their rate of change is slower is comparison to their fast TV counterparts. Greater fidelity can be achieved with higher order parametric functions which yield more numerous and increasingly slower parameters. Considering the exponential rate of rise in the number of calculations to be performed as a function of parameters, a good compromise should be achieved by considering the available processing power and desired control accuracy. A very good demonstration of this principle can be found in [37] with FL control.

2) DIGITAL SLIDING MODE CONTROL

As described in Section VII, sliding mode control offers great flexibility in defining the nature of the desired dynamic response. Yet, similar to other techniques, the equivalent control law in sliding mode control cannot be realised without model information. For lower fidelity models, the contribution of disturbance rejection term is improved which also results into sub-optimal control performance. A very effective solution to this issue is presented in the form of a 'digital sliding mode control design' in [87]. Under this approach a part of unmodelled dynamics can be calculated in the form

of a unit sample delayed disturbance. Thus, net magnitude of the discontinuous switching term can be greatly reduced.

3) HYBRID CONTROL TECHNIQUES

Although the fixed gain PI control is insufficient in terms of maintaining consistency in dynamic response throughout the conduction period, it is very inexpensive in terms of computation and memory requirement. A combined solution of PI+delta modulation [88] have proved to be a practically viable solution. This concept can promisingly yield a more robust controller with incorporation of the principles of sliding mode control in the design process.

B. CONCLUDING REMARK

The primary motivation behind all the analytical treatments presented in this paper is to summarize the knowledge behind a good engineering judgment necessary for the selection of an appropriate control technique for a fixed switching frequency SRM drive in the application of interest and the exploration of further possibilities in the improvement of its performance and hence, the candidacy for an ever-widening array of applications.

REFERENCES

[1] M. Krishnamurthy, C. S. Edrington, A. Emadi, P. Asadi, M. Ehsani, and B. Fahimi, "Making the case for applications of switched reluctance motor technology in automotive products," *IEEE Trans. Power Electron.*, vol. 21, no. 3, pp. 659–675, May 2006.

[2] R. Krishnan, *Switched Reluctance Motor Drives: Modeling, Simulation, Analysis, Design, and Applications*. Boca Raton, FL, USA: CRC Press, 2017.

[3] B. Bilgin, J. W. Jiang, and A. Emadi, *Switched Reluctance Motor Drives: Fundamentals to Applications*. Boca Raton, FL, USA: CRC Press, 2019.

[4] A. Radun, "Generating with the switched reluctance motor," in *Proc. IEEE Appl. Power Electron. Conf. Expo. (ASPEC)*, vol. 1, Feb. 1994, pp. 41–47.

[5] E. Richter, "High temperature, lightweight, switched reluctance motors and generators for future aircraft engine applications," in *Proc. Amer. Control Conf.*, Jun. 1988, pp. 1846–1851.

[6] E. Richter and C. Ferreira, "Performance evaluation of a 250 kW switched reluctance starter generator," in *Proc. Conf. Rec. IEEE Ind. Appl. Conf. 30th IAS Annu. Meeting (IAS)*, vol. 1, Oct. 1995, pp. 434–440.

[7] H. Chen and C. Pavlitov, "Large power analysis of switched reluctance machine system for coal mine," *Mining Sci. Technol. China*, vol. 19, no. 5, pp. 657–659, Sep. 2009.

[8] C. Pollock and C.-Y. Wu, "Acoustic noise cancellation techniques for switched reluctance drives," *IEEE Trans. Ind. Appl.*, vol. 33, no. 2, pp. 477–484, Mar. 1997.

[9] J. Ye, B. Bilgin, and A. Emadi, "An offline torque sharing function for torque ripple reduction in switched reluctance motor drives," *IEEE Trans. Energy Convers.*, vol. 30, no. 2, pp. 726–735, Jun. 2015.

[10] H. Li, B. Bilgin, and A. Emadi, "An improved torque sharing function for torque ripple reduction in switched reluctance machines," *IEEE Trans. Power Electron.*, vol. 34, no. 2, pp. 1635–1644, Feb. 2019.

[11] Q. Sun, J. Wu, C. Gan, Y. Hu, and J. Si, "OCTSF for torque ripple minimisation in SRMs," *IET Power Electron.*, vol. 9, no. 14, pp. 2741–2750, Nov. 2016.

[12] J. Ye, B. Bilgin, and A. Emadi, "An extended-speed low-ripple torque control of switched reluctance motor drives," *IEEE Trans. Power Electron.*, vol. 30, no. 3, pp. 1457–1470, Mar. 2015.

[13] R. B. Inderka and R. W. A. A. De Doncker, "High-dynamic direct average torque control for switched reluctance drives," *IEEE Trans. Ind. Appl.*, vol. 39, no. 4, pp. 1040–1045, Jul. 2003.

[14] A. Klein-Hessling, A. Hofmann, and R. W. De Doncker, "Direct instantaneous torque and force control: A control approach for switched reluctance machines," *IET Electr. Power Appl.*, vol. 11, no. 5, pp. 935–943, May 2017.

[15] R. B. Inderka and R. W. De Doncker, "DITC-direct instantaneous torque control of switched reluctance drives," *IEEE Trans. Ind. Appl.*, vol. 39, no. 4, pp. 1046–1051, Jul. 2003.

[16] R. Mikail, I. Husain, Y. Sozer, M. S. Islam, and T. Sebastian, "A fixed switching frequency predictive current control method for switched reluctance machines," *IEEE Trans. Ind. Appl.*, vol. 50, no. 6, pp. 3717–3726, Nov. 2014.

[17] X. Li and P. Shamsi, "Model predictive current control of switched reluctance motors with inductance auto-calibration," *IEEE Trans. Ind. Electron.*, vol. 63, no. 6, pp. 3934–3941, Jun. 2016.

[18] R. Tarvirdilu-Asl, S. Nalakath, B. Bilgin, and A. Emadi, "A finite control set model predictive torque control for switched reluctance motor drives with adaptive turn-off angle," in *Proc. 45th Annu. Conf. IEEE Ind. Electron. Soc. (IECON)*, vol. 1, Oct. 2019, pp. 840–845.

[19] D. F. Valencia, S. R. Filho, A. D. Callegaro, M. Preindl, and A. Emadi, "Virtual-flux finite control set model predictive control of switched reluctance motor drives," in *Proc. 45th Annu. Conf. IEEE Ind. Electron. Soc.*, vol. 1, Oct. 2019, pp. 1465–1470.

[20] S. Wang, "Conductive EMI issues in power electronics systems," in *Proc. IEEE Int. Symp. Electromagn. Compat. Signal/Power Integrity (EMCSI)*, Aug. 2017, pp. 1–110.

[21] K. Vijayakumar, R. Karthikeyan, S. Paramasivam, R. Arumugam, and K. N. Srinivas, "Switched reluctance motor modeling, design, simulation, and analysis: A comprehensive review," *IEEE Trans. Magn.*, vol. 44, no. 12, pp. 4605–4617, Dec. 2008.

[22] S. Li, S. Zhang, T. G. Habetler, and R. G. Harley, "Modeling, design optimization, and applications of switched reluctance machines—A review," *IEEE Trans. Ind. Appl.*, vol. 55, no. 3, pp. 2660–2681, Feb. 2019.

[23] X. D. Xue, K. W. E. Cheng, and S. L. Ho, "Optimization and evaluation of torque-sharing functions for torque ripple minimization in switched reluctance motor drives," *IEEE Trans. Power Electron.*, vol. 24, no. 9, pp. 2076–2090, Sep. 2009.

[24] R. Abdel-Fadil, F. Al-Amyal, and L. Számel, "Torque ripples minimization strategies of switched reluctance motor-a review," in *Proc. Int. IEEE Conf. Workshop Óbuda Elect. Power Eng. (CANDO-EPE)*, Nov. 2019, pp. 41–46.

[25] M. V. de Paula, T. A. dos Santos Barros, and P. J. D. S. Neto, "A review of classic torque control techniques for switched reluctance motors," in *Modelling and Control of Switched Reluctance Machines*. London, U.K.: IntechOpen, 2020.

[26] A. Y. Anekunu, S. P. Chowdhury, and S. Chowdhury, "A review of research and development on switched reluctance motor for electric vehicles," in *Proc. IEEE Power Energy Soc. Gen. Meeting*, Jul. 2013, pp. 1–5.

[27] D. Susitra, E. Jebaseeli, E. Annie, and S. Paramasivam, "Switched reluctance generator-modeling, design, simulation, analysis and control a comprehensive review," *Int. J. Comput. Appl.*, vol. 1, no. 2, pp. 10–16, 2010.

[28] X. Gao, X. Wang, Z. Li, and Y. Zhou, "A review of torque ripple control strategies of switched reluctance motor," *Int. J. Control Autom.*, vol. 8, no. 4, pp. 103–116, Apr. 2015.

[29] X. Rain, M. Hilairet, and O. Bethoux, "Comparative study of various current controllers for the switched reluctance machine," in *Proc. IEEE Vehicle Power Propuls. Conf.*, Lille, France, Sep. 2010, pp. 1–6. [Online]. Available: https://hal.archives-ouvertes.fr/hal-02054625

[30] J. Taylor, D. F. Valencia, B. Bilgin, M. Narimani, and A. Emadi, "Comparison of current control strategies for low-and high-power switched reluctance motor drives," in *Proc. IEEE Transp. Electrific. Conf. Expo (ITEC)*, Jun. 2020, pp. 198–203.

[31] J.-W. Choi and S.-K. Sul, "Inverter output voltage synthesis using novel dead time compensation," *IEEE Trans. Power Electron.*, vol. 11, no. 2, pp. 221–227, Mar. 1996.

[32] T.-I. Kim, J.-S. Han, T.-H. Oh, Y.-S. Kim, S.-H. Lee, and D.-I. D. Cho, "A new accurate discretization method for high-frequency component mechatronics systems," *Mechatronics*, vol. 62, Oct. 2019, Art. no. 102250.

[33] M. Ilic-Spong, T. J. E. Miller, S. R. Macminn, and J. S. Thorp, "Instantaneous torque control of electric motor drives," *IEEE Trans. Power Electron.*, vol. PE-2, no. 1, pp. 55–61, Jan. 1987.

[34] M. Ilic-Spong, R. Marino, S. Peresada, and D. Taylor, "Feedback linearizing control of switched reluctance motors," *IEEE Trans. Autom. Control*, vol. 32, no. 5, pp. 371–379, May 1987.

[35] A. Isidori, *Nonlinear Control Systems*. London, U.K.: Springer, 2013.

[36] S. K. Panda and P. K. Dash, "Application of nonlinear control to switched reluctance motors: A feedback linearisation approach," *IEE Proc. Electr. Power Appl.*, vol. 143, no. 5, pp. 371–379, Sep. 1996.
[37] L. B. Amor, L.-A. Dessaint, O. Akhrif, and G. Olivier, "Adaptive input-output linearization of a switched reluctance motor for torque control," in *Proc. 19th Annu. Conf. IEEE Ind. Electron. (IECON)*, Nov. 1993, pp. 2155–2160.
[38] C. A. Jacobson, A. M. Stankovic, G. Tadmor, and Z. Coric, "A family of robust control strategies for switched reluctance motors," in *Proc. Int. Conf. Power Electron. Drive Syst. (PEDS)*, 1995, pp. 192–197.
[39] D. G. Taylor, "Improved pulse-width modulated control of switched reluctance motors," in *Proc. Amer. Control Conf.*, May 1990, pp. 2083–2088.
[40] C. Gan, J. Wu, Q. Sun, S. Yang, Y. Hu, and L. Jin, "Low-cost direct instantaneous torque control for switched reluctance motors with bus current detection under soft-chopping mode," *IET Power Electron.*, vol. 9, no. 3, pp. 482–490, Mar. 2016.
[41] R. Cardenas, R. Pena, M. Perez, J. Clare, G. Asher, and P. Wheeler, "Control of a switched reluctance generator for variable-speed wind energy applications," *IEEE Trans. Energy Convers.*, vol. 20, no. 4, pp. 781–791, Dec. 2005.
[42] H.-K. Bae, B.-S. Lee, P. Vijayraghavan, and R. Krishnan, "A linear switched reluctance motor: Converter and control," *IEEE Trans. Ind. Appl.*, vol. 36, no. 5, pp. 1351–1359, Sep. 2000.
[43] Z. Lin, D. Reay, B. Williams, and X. He, "High-performance current control for switched reluctance motors based on on-line estimated parameters," *IET Electr. Power Appl.*, vol. 4, no. 1, pp. 67–74, Jan. 2010.
[44] S. E. Schulz and K. M. Rahman, "High-performance digital PI current regulator for EV switched reluctance motor drives," *IEEE Trans. Ind. Appl.*, vol. 39, no. 4, pp. 1118–1126, Jul. 2003.
[45] H. Hannoun, M. Hilairet, and C. Marchand, "High performance current control of a switched reluctance machine based on a gain-scheduling PI controller," *Control Eng. Pract.*, vol. 19, no. 11, pp. 1377–1386, Nov. 2011.
[46] S. Chowdhuri, S. Biswas, and A. Mukherjee, "Performance studies of fuzzy logic based PI-like controller designed for speed control of switched reluctance motor," in *Proc. 1st IEEE Conf. Ind. Electron. Appl.*, May 2006, pp. 1–5.
[47] S.-C. Wang and Y.-H. Liu, "A modified PI-like fuzzy logic controller for switched reluctance motor drives," *IEEE Trans. Ind. Electron.*, vol. 58, no. 5, pp. 1812–1825, May 2011.
[48] E. Karakas and S. Vardarbasi, "Speed control of SR motor by self-tuning fuzzy PI controller with artificial neural network," *Sadhana*, vol. 32, no. 5, pp. 587–596, Oct. 2007.
[49] S. S. Ahmad and G. Narayanan, "Linearized modeling of switched reluctance motor for closed-loop current control," *IEEE Trans. Ind. Appl.*, vol. 52, no. 4, pp. 3146–3158, Jul. 2016.
[50] J. Dannehl, F. W. Fuchs, S. Hansen, and P. B. Thøgersen, "Investigation of active damping approaches for PI-based current control of grid-connected pulse width modulation converters with LCL filters," *IEEE Trans. Ind. Appl.*, vol. 46, no. 4, pp. 1509–1517, Jul. 2010.
[51] G. Frobenius, *Verallgemeinerung des Sylow'schen satzes*. Berlin, Germany: Reimer, 1895.
[52] A. Rajendran and S. Padma, "H-infinity robust control technique for controlling the speed of switched reluctance motor," *Frontiers Electr. Electron. Eng.*, vol. 7, no. 3, pp. 337–346, Sep. 2012.
[53] G. Rigatos, P. Siano, and S. Ademi, "Nonlinear H-infinity control for switched reluctance machines," *Nonlinear Eng.*, vol. 9, no. 1, pp. 14–27, Jul. 2019.
[54] N. Ouddah, M. Boukhnifer, A. Chaibet, E. Monmasson, and E. Berthelot, "Experimental robust H_∞ controller design of switched reluctance motor for electrical vehicle application," in *Proc. IEEE Conf. Control Appl. (CCA)*, Oct. 2014, pp. 1570–1575.
[55] S. Fadhel, I. Bahri, and M. Zhang, "H-infinity controller design for the switched reluctance machine," *Int. J. Mech. Mechtron. Eng.*, vol. 11, no. 1, pp. 132–141, 2017. [Online]. Available: https://publications.waset.org/vol/121
[56] B. A. Francis, *Lecture Notes in Control and Information Sciences*. Berlin, Germany: Springer-Verlag, 1987.
[57] A. Sadeghzadeh and B. Araabi, "Auto-tune predictive control of switched reluctance motor," in *Proc. IEEE Int. Symp. Ind. Electron.*, vol. 1, Jul. 2006, pp. 335–340.
[58] X. Li and P. Shamsi, "Inductance surface learning for model predictive current control of switched reluctance motors," *IEEE Trans. Transport. Electrific.*, vol. 1, no. 3, pp. 287–297, Oct. 2015.
[59] S. S. Ahmad and G. Narayanan, "Predictive control based constant current injection scheme for characterization of switched reluctance machine," *IEEE Trans. Ind. Appl.*, vol. 54, no. 4, pp. 3383–3392, Jul. 2018.
[60] R. E. Kalman, "On the general theory of control systems," in *Proc. 1st Int. Conf. Automat. Control*, Moscow, Russia, Aug. 1960, pp. 481–492.
[61] H. A. Alharkan, S. Saadatmand, M. Ferdowsi, and P. Shamsi, "Optimal tracking current control of switched reluctance motor drives using reinforcement Q-learning scheduling," 2020, *arXiv:2006.07764*. [Online]. Available: https://arxiv.org/abs/2006.07764
[62] B. D. Anderson and J. B. Moore, *Optimal Control: Linear Quadratic Methods*. North Chelmsford, MA, USA: Courier Corporation, 2007.
[63] D. E. Kirk, *Optimal Control Theory: An Introduction*. North Chelmsford, MA, USA: Courier Corporation, 2004.
[64] B. Kiumarsi-Khomartash, F. L. Lewis, M.-B. Naghibi-Sistani, and A. Karimpour, "Optimal tracking control for linear discrete-time systems using reinforcement learning," in *Proc. 52nd IEEE Conf. Decis. Control*, Dec. 2013, pp. 3845–3850.
[65] E. Eweda and O. Macchi, "Convergence of the RLS and LMS adaptive filters," *IEEE Trans. Circuits Syst.*, vol. 34, no. 7, pp. 799–803, Jul. 1987.
[66] R. M. Johnstone, C. R. Johnson, R. R. Bitmead, and B. D. O. Anderson, "Exponential convergence of recursive least squares with exponential forgetting factor," *Syst. Control Lett.*, vol. 2, no. 2, pp. 77–82, Aug. 1982.
[67] Y. Haiqing, S. K. Panda, and L. Y. Chii, "Performance comparison of sliding mode control with PI control for four-quadrant operation of switched reluctance motors," in *Proc. Int. Conf. Power Electron., Drives Energy Syst. Ind. Growth*, vol. 1, Jan. 1996, pp. 381–387.
[68] J. Ye, P. Malysz, and A. Emadi, "A fixed-switching-frequency integral sliding mode current controller for switched reluctance motor drives," *IEEE J. Emerg. Sel. Topics Power Electron.*, vol. 3, no. 2, pp. 381–394, Jun. 2015.
[69] W. Shang, S. Zhao, Y. Shen, and Z. Qi, "A sliding mode flux-linkage controller with integral compensation for switched reluctance motor," *IEEE Trans. Magn.*, vol. 45, no. 9, pp. 3322–3328, Sep. 2009.
[70] F. B. Salem, I. Bahri, H. Maamri, and N. Derbel, "A second-order sliding mode control of switched reluctance motor," *Electr. Power Compon. Syst.*, vol. 48, nos. 6–7, pp. 640–651, Apr. 2020.
[71] M. Rafiq, S.-U. Rehman, F.-U. Rehman, Q. R. Butt, and I. Awan, "A second order sliding mode control design of a switched reluctance motor using super twisting algorithm," *Simul. Model. Pract. Theory*, vol. 25, pp. 106–117, Jun. 2012.
[72] M. Divandari, B. Rezaie, and E. Amiri, "Robust speed control of switched reluctance motor drive based on full order terminal sliding mode control," in *Proc. IEEE Appl. Power Electron. Conf. Expo. (APEC)*, Mar. 2020, pp. 2423–2428.
[73] Y. Shtessel, C. Edwards, L. Fridman, and A. Levant, *Sliding Mode Control and Observation*. New York, NY, USA: Springer, 2014.
[74] D. G. Taylor, "Adaptive control design for a class of doubly-salient motors," in *Proc. 30th IEEE Conf. Decis. Control*, Dec. 1991, pp. 2903–2908.
[75] S. A. Bortoff, R. R. Kohan, and R. Milman, "Adaptive control of variable reluctance motors: A spline function approach," *IEEE Trans. Ind. Electron.*, vol. 45, no. 3, pp. 433–444, Jun. 1998.
[76] F. Peng, J. Ye, and A. Emadi, "A digital PWM current controller for switched reluctance motor drives," *IEEE Trans. Power Electron.*, vol. 31, no. 10, pp. 7087–7098, Dec. 2015.
[77] L. Szamel, "Model reference adaptive control of SRM drives," in *Proc. 10th Int. Power Electron. Motion Control Conf. (EPE-PEMC)*, Cavtat, Croatia, 2002, p. 466.
[78] H. Naitoh and H. Ishikawa, "A current controller for a switched reluctance motor based on model reference adaptive control," in *Proc. SPEEDAM*, Jun. 2010, pp. 1270–1275.
[79] K. J. Åström, "Adaptive control," in *Mathematical System Theory*. New York, NY, USA: Springer, 1991, pp. 437–450.
[80] G. Espinosa-Pérez, P. Maya-Ortiz, M. Velasco-Villa, and H. Sira-Ramírez, "Passivity-based control of switched reluctance motors with nonlinear magnetic circuits," *IEEE Trans. Control Syst. Technol.*, vol. 12, no. 3, pp. 439–448, May 2004.
[81] M. M. N. Isfahani, S. M. Saghaian-Nejad, A. Rashidi, and H. A. Zarchi, "Passivity-based adaptive sliding mode speed control of switched reluctance motor drive considering torque ripple reduction," in *Proc. IEEE Int. Electric Mach. Drives Conf. (IEMDC)*, May 2011, pp. 1480–1485.
[82] S. Boyd and S. S. Sastry, "Necessary and sufficient conditions for parameter convergence in adaptive control," *Automatica*, vol. 22, no. 6, pp. 629–639, Nov. 1986.

[83] S. K. Sahoo, S. K. Panda, and J. X. Xu, "Iterative learning-based high-performance current controller for switched reluctance motors," *IEEE Trans. Energy Convers.*, vol. 19, no. 3, pp. 491–498, Sep. 2004.
[84] X. Zhang, Q. Yang, M. Ma, Z. Lin, and S. Yang, "A switched reluctance motor torque ripple reduction strategy with deadbeat current control and active thermal management," *IEEE Trans. Veh. Technol.*, vol. 69, no. 1, pp. 317–327, Jan. 2020.
[85] T. Zhao, Y. Wu, and X. Gui, "A modified current predict controll with incremental inductance and resistance self-learning for switched reluctance machines," in *Proc. 22nd Int. Conf. Electr. Mach. Syst. (ICEMS)*, Aug. 2019, pp. 1–6.
[86] K. Tsakalis and P. Ioannou, "Adaptive control of linear time-varying plants," *Automatica*, vol. 23, no. 4, pp. 459–468, Jul. 1987.
[87] S. V. Drakunov and V. Utkin, "On discrete-time sliding modes," in *Nonlinear Control Systems Design 1989*. Amsterdam, The Netherlands: Elsevier, 1990, pp. 273–278.
[88] G. Gallegos-López and K. Rajashekara, "Peak PWM current control of switched reluctance and AC machines," in *Proc. Conf. Rec. IEEE Ind. Appl. Conf. 37th IAS Annu. Meeting*, vol. 2, Oct. 2002, pp. 1212–1218.

SUMEDH DHALE (Student Member, IEEE) received the B.E. degree in electrical engineering from the University of Pune, Pune, in 2012, and the M.Tech. degree in power electronics and drives from VIT University, Vellore, in 2015. He is currently pursuing the Ph.D. degree in electrical and computer engineering with McMaster University, Hamilton, ON, Canada.

His areas of research include the control and estimation of electric drives and power converters.

BABAK NAHID-MOBARAKEH (Senior Member, IEEE) received the Ph.D. degree in electrical engineering from the Institut National Polytechnique de Lorraine (INPL), France, in 2001.

From 2001 to 2006, he was with the University of Picardie Jules Verne, Amiens, France, as an Assistant Professor and then an Associate Professor. In September 2006, he joined the École Nationale Súperieure d'Électricité et de Mécanique, University of Lorraine, Nancy, France, as an Associate Professor, where he became a Full Professor, in 2016. Since January 2020, he has been with McMaster University, Hamilton, ON, Canada, as a Professor in electrical engineering. He is the author or coauthor of over 300 international peer reviewed journal and conference papers as well as several book chapters and patents. His main research interests include nonlinear and robust control design of power converters and drives, fault detection and fault-tolerant control of motor drives, and design, control, and stabilization of microgrids. He was a recipient of several IEEE awards. He was the General Co-Chair of the 2020 IEEE Transportation Electrification Conference and Expo (ITEC). From 2012 to 2019, he served as the Secretary, Vice Chair, Chair, and Past Chair for the Industrial Automation and Control Committee (IACC) of the IEEE Industry Applications Society (IAS). He is currently the Vice Chair of the IEEE Power Electronics Society (PELS) TC4 "Electrical Transportation Systems."

ALI EMADI (Fellow, IEEE) received the B.S. and M.S. degrees (Hons.) in electrical engineering from the Sharif University of Technology, Tehran, Iran, in 1995 and 1997, respectively, and the Ph.D. degree in electrical engineering from Texas A&M University, College Station, TX, USA, in 2000. He is currently the Canada Excellence Research Chair Laureate at McMaster University, Hamilton, ON, Canada. He is also the NSERC/FCA Industrial Research Chair in Electrified Powertrains and the Tier I Canada Research Chair in Transportation Electrification and Smart Mobility. Before joining McMaster University, he was the Harris Perlstein Endowed Chair Professor of Engineering and the Director of the Electric Power and Power Electronics Center and the Grainger Laboratories, Illinois Institute of Technology, Chicago, where he established research and teaching facilities as well as courses in power electronics, motor drives, and vehicular power systems. He was the Founder, Chairman, and President of Hybrid Electric Vehicle Technologies (HEVT), Inc.,—a university spin-off company of Illinois Tech. He is currently the President and Chief Executive Officer of Enedym Inc., and Menlolab Inc.,—spin-off companies of McMaster University. He is the principal author/coauthor of over 500 journal and conference papers as well as several books, including *Vehicular Electric Power Systems* (2003), *Energy-Efficient Electric Motors* (2004), *Uninterruptible Power Supplies and Active Filters* (2004), *Modern Electric, Hybrid Electric, and Fuel Cell Vehicles* (2nd Edition, 2009), and *Integrated Power Electronic Converters and Digital Control* (2009). He is also an Editor of the *Handbook of Automotive Power Electronics and Motor Drives* (2005) and *Advanced Electric Drive Vehicles* (2014). He is a Co-Editor of *Switched Reluctance Motor Drives* (2018). He was the Inaugural General Chair of the 2012 IEEE Transportation Electrification Conference and Expo (ITEC) and has chaired several IEEE and SAE conferences in the areas of vehicle power and propulsion. He was the founding Editor-in-Chief of the IEEE TRANSACTIONS ON TRANSPORTATION ELECTRIFICATION, from 2014 to 2020.